Single Event Burnout in Homojunction GaN Vertical PiN Diodes with Hybrid Edge Termination Design

A. S. Senarath[1], S. Islam[1], A. Sengupta[2], M. W. McCurdy[2], T. Anderson[3], A. Jacobs[3], R. Kaplar[4], D. R. Ball[2], E. X. Zhang[5], S. T. Pantelides[2,6], R. A. Reed[2], M. A. Ebrish[2], D. M. Fleetwood[2], J. D. Caldwell[7], and R. D. Schrimpf[2]

[1]*Interdisciplinary Materials Science Program, Vanderbilt University, Nashville, TN 37235, USA*
[2]*Department of Electrical and Computer Engineering, Vanderbilt University, Nashville, TN 37235, USA*
[3]*Power Electronics Branch, Naval Research Laboratory, Washington, DC 20375, USA*
[4]*Semiconductor Material and Device Sciences Department, Sandia National Laboratories, Albuquerque, NM 87123, USA*
[5]*Department of Electrical and Computer Engineering, University of Central Florida, Orlando, FL 32816, USA*
[6]*Department of Physics and Astronomy, Vanderbilt University, Nashville, TN 37235, USA*
[7]*Department of Mechanical Engineering, Vanderbilt University, Nashville, TN 37235, USA*

ABSTRACT

GaN devices play a major role in modern electronics, providing high-power handling, efficient high-frequency operation, and resilience in harsh environments. However, electric field crowding at the edge of the anode often limits its full potential, leading to single-event effects (SEEs) at lower bias voltages under heavy ion radiation. Here, we report on the performance of homojunction GaN vertical PiN diodes with a hybrid-edge-termination design under heavy ion irradiation, specifically, oxygen ions, chlorine ions, Cf-252 fission fragments, and alpha particles from an Am-241 source. The unique hybrid edge termination (HET) design provides better electric field management, preventing breakdown from occurring at the edge of the anode at lower voltages. The results of this study reveal that these devices exhibit excellent tolerance to 12-MeV oxygen and 16-MeV chlorine ions, owing to their low linear energy transfer (LET) and range in GaN. However, single-event burnout (SEB) is observed during the Cf-252 exposure at about 50% of the diodes' electrical breakdown voltage due to the presence of higher LET and longer-range ions. Optical and scanning electron microscopy (SEM) reveal that the damage that caused by SEB lies close to the center of these devices rather than the anode edge. Devices with junction termination extension (JTE) instead of HET edge termination also show similar SEB when irradiated with Cf-252 fission fragments. Physical damage due to SEB occurs at the edge of the anode for these devices. These comparative results show the benefits of HET for enhancing the resistance of GaN-based PiN diodes to heavy-ion irradiation.

In recent years, gallium nitride (GaN) has emerged as a highly promising material for power electronic applications owing to its distinctive characteristics, including a wide band gap, high electron mobility, and robust electrical properties[1,2,3]. With a band gap of 3.4 eV, GaN devices offer significant advantages over traditional silicon-based technologies, such as increased efficiency, rapid switching speeds, and elevated power density[4,5,6]. Consequently, GaN technology has garnered prominence across various sectors, particularly in space applications[7].

Despite its promising attributes, the susceptibility of GaN devices to radiation-induced single-event effects (SEEs) remains a significant concern, necessitating voltage derating and impacting overall reliability[8,9]. For a long time, the quality of native GaN substrates was an inherent challenge for the advancement of vertical GaN devices, leading to a primary focus on GaN-on-Si and GaN-on-SiC devices in radiation effect studies[10]. However, the growth of thick GaN layers on non-GaN substrates is hindered by high dislocation/defect densities resulting from lattice mismatches and differences in thermal expansion coefficients[11,12]. Also, in lateral GaN devices, enhancing breakdown voltage and improving the SEE response necessitates an increase in lateral device dimensions[13]. Conversely, in vertical GaN power devices, the capacity to withstand high voltages relies on a thick, lightly doped drift layer, which is much more convenient and effective[14].

Recent developments in fabricating high-quality GaN substrates have sparked renewed interest in vertical low dislocation/defect density GaN devices for high-power and radiation environment applications[15]. Mature technologies like silicon carbide (SiC) employ PiN diode structures that have comparably well-understood radiation responses[16]. The radiation hardness of GaN PiN diode structures remains less understood due to a lack of vertical GaN PiN diodes. Moreover, the phenomenon of electric field crowding at the edge of the anode, leading to breakdown at lower reverse voltages before reaching the maximum potential of the material, is common across all high-power devices[17,17,18,19]. To mitigate this issue, various edge termination structures, including junction termination extension (JTE), hybrid edge termination (HET), and bevel edge termination, have been developed[20,21]. While some structures like bevel edge termination demonstrate improved electric field distribution, their complex fabrication processes and tool requirements limit mass manufacturing suitability. In contrast, hybrid edge termination presents a promising alternative that does not require specialized tools or complex fabrication steps[20].

Here, we investigate single-event burnout in homojunction GaN vertical PiN diodes fabricated on native GaN substrates with HET. Results from a similar device with JTE edge termination are presented as a baseline device for comparison. We studied the electrical performance of vertical GaN PiN diodes, characterized by high quality and low threading-dislocation density (TDD) within the 10^4-10^6 cm^{-2} range[22]. Metal-organic chemical vapor deposition (MOCVD) was employed to grow Mg-doped GaN layers with a thickness of 400 nm, with a targeted doping level of 2×10^{19} cm^{-3}. These epitaxial layers were grown atop a lightly doped n-type hydride phase vapor epitaxy (HPVE) layer, which had a thickness of 8 µm and a targeted doping concentration of 1×10^{16} cm^{-3}. The TDD in this layer lies within the 10^4 to 10^6 cm^{-2} range. To make an ohmic contact, the top region of the anode was doped with 2×10^{20} cm^{-3} Mg. The cross-section of the device with doping densities and thicknesses of different layers is shown in Fig. 1(a).

A junction termination extension and guard rings (JTE/GR) hybrid structure was integrated through nitrogen implantation. The hybrid configuration incorporates alternating deep and shallow charge-compensating implants, as illustrated in the cross-section in Fig. 1(c). The geometric design of this hybrid structure has been demonstrated to exhibit superior electric field management and enhanced breakdown voltage[20,21]. These devices were specifically engineered for high-power electronics applications; the experimental electrical breakdown

voltage reached approximately 700 V in an ambient air environment and around 950 V in vacuum conditions[23,20,24]. To assess the efficacy of the HET, additional devices featuring the JTE edge termination were subjected to testing. The cross-section of the JTE edge termination design is similar to the devices with HET and is depicted in Fig. 1(a). A cross-section of the JTE edge termination region is shown in Fig.1(d). However, they differ in terms of a targeted anode doping density of 1×10^{16} cm^{-3}, a 500 nm anode thickness, and the utilization of the JTE edge termination design instead of HET. The current-voltage (IV) characteristics of both device types are presented in Fig. 1(b). Notably, devices with a JTE edge termination design exhibit lower leakage currents compared to their HET counterparts, which is attributed to the lower anode doping density and thicker anode region[23,24]. However, these differences in doping density and thickness will not affect the main point of this study, which is the radiation sensitivity of the edge of the anode region. It is essential to note that all devices utilized in this investigation share a consistent 0.105 mm^2 anode area.

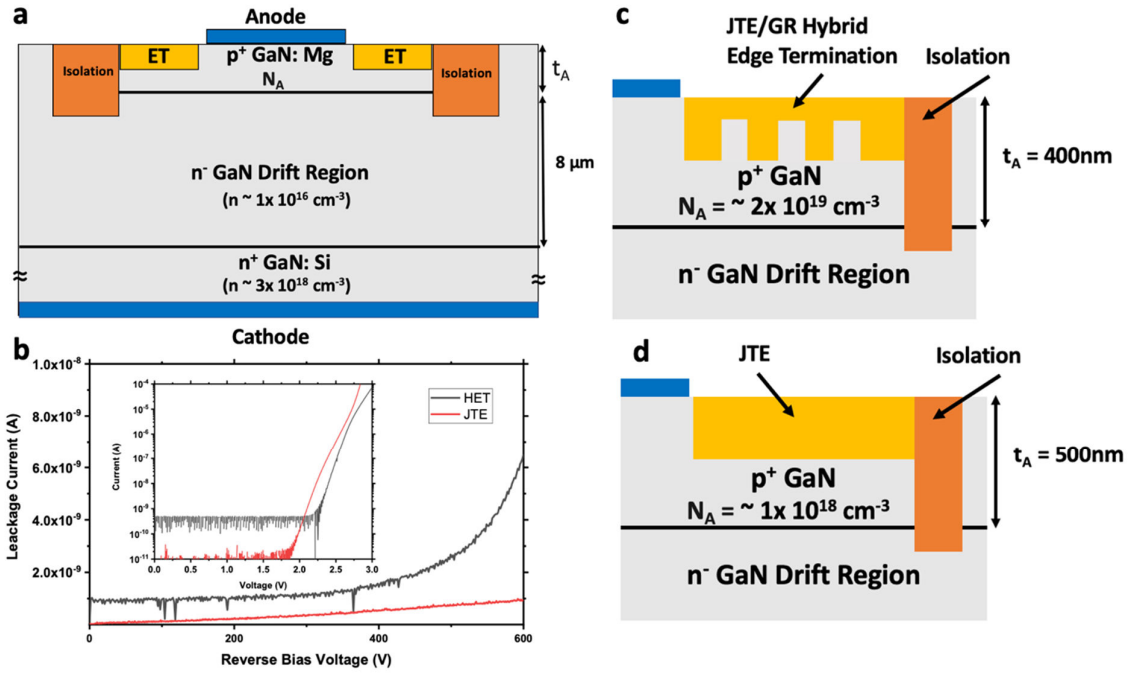

FIG 1: Device structure of homojunction GaN vertical PiN diodes: (a) device cross-section, (b) forward and reverse IV characteristics for two types of the devices, (c) cross-section of the hybrid edge termination region, and (d) cross-section of the junction termination extension region.

The radiation damage that causes SEB often occurs close to the edge of the anode due to electric field crowding at that region [25,18,19]. Previous work shows that improved electric-field management at the edge of devices enables higher SEB threshold voltage for vertical β-Ga_2O_3 Schottky diodes[26]. This work investigates whether better field management by an efficient HET design can reduce the radiation sensitivity of the edge of the anode compared to the JTE edge termination design and prevent low-voltage SEB by anode edge damage. For that investigation, we used oxygen and chlorine ions to represent two different linear energy transfer (LET) ions in space.[27] Also, we used a Cf-252 button source to represent a combination of high and low LET heavy ions[26,28].

TABLE I. PROPERTIES OF DIFFERENT IONS USED IN THIS STUDY.

Source	Energy (MeV)	LET(MeV-cm^2/mg)	Range (μm)
Oxygen	12	5.3	4.9
Chlorine	16	12.0	3.9
0.86 μCi Cf-252	5.9(Alpha particles) 102.5 and 78.7 (mean energies for fission fragments)[29]	42-45 (Mean)[28]	~14 (Mean)[28]
0.1 μCi Am-241	5.4(Alpha particles)	<1[18]	>10 [18]

The respective energies, LET values, and ion ranges in GaN of the ions used in this study are presented in Table 1. Oxygen and chlorine heavy ion experiments were conducted at Vanderbilt University's Pelletron facility. Vacuum-sealed diodes were subjected to an ion flux of 5×10^5 ions/cm^2/s of either 12-MeV oxygen or 16-MeV chlorine ions. SRIM calculations show that a 12-MeV oxygen ion has a surface LET of 5.3 MeV-cm^2/mg and an approximate range of 4.9 μm. A 16-MeV chlorine ion has a surface LET of 12.0 MeV-cm^2/mg and a range of approximately 3.9 μm in GaN [30]. Table 1 also shows the mean energy, LET, and range of the 0.86 μCi Cf -252 source and the 0.1 μCi Am-241 source used in this study. Alpha particle irradiation and Cf-252 fission fragment irradiation were done under ambient air conditions.

Sequential irradiation for a range of reverse bias voltages was conducted, beginning at 200 V for oxygen ions and continuing in 25 V increments to progressively greater reverse biases until the device exhibited catastrophic breakdown. The IV characteristics of devices P1-P4 used for the oxygen ion irradiation are shown in Fig S1, showing that all devices behave similarly before irradiation. First, the device was allowed to settle for 10 s before activating the ion beam for every exposure. The device did not show any change in current when the beam was turned on and off. Following an exposure of 100 s, the beam was switched off. Device failure in this study is defined as the point that the diode current approaches the 1.0 mA power supply compliance setting. The change in leakage current for 650 V to 775 V sequential irradiation of device P3 is shown in Fig. 2(a). At 775 V reverse bias, the device exhibited catastrophic breakdown ~75 s after turning the beam on, as confirmed by the post-rad forward and reverse characteristics. Clear damage is observed close to the edge of the anode, as shown in the optical image in Fig 2(b). Four similar devices were tested using the same procedure; the average breakdown voltage is 800.0 ± 20.0 V, which is in the range of the breakdown voltage in the absence of ion irradiation [see Table SI in the supplementary material].

The same experiment was performed using chlorine ions, and similar trends were observed. Again, four devices (P5-P8) were tested with chlorine ions, and the average breakdown voltage was 812.5 ± 59.5 V. [See Fig S2, Fig S3, and Table SII in the supplementary material]. That value is also in the range of the breakdown voltage of these devices in the absence of heavy ions. Also, the physical damage is always at the edge of the anode, and looks similar to damage from the electrical breakdown of this kind of device. Therefore, these results suggest that the oxygen and chlorine ions do not have much effect on the device. This resilience can be attributed to the relatively low LET and short ranges of these ions in GaN relative to the 8 μm thickness of the drift layer, which exhibits the most SEB sensitivity within the device.

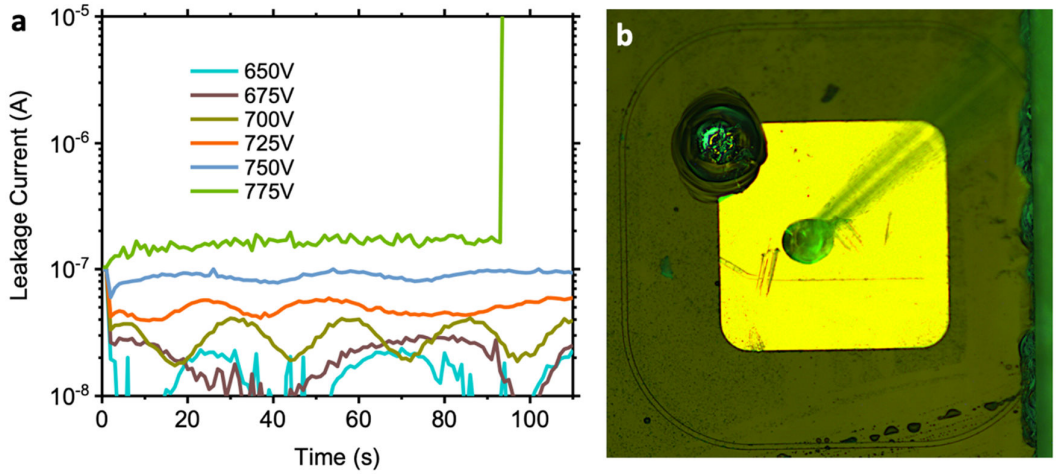

FIG 2: Change in leakage current during oxygen ion irradiation at different voltages of a device with HET (a) and optical image of the damaged device (b).

Similar devices were irradiated with Cf-252 fission fragments, which are often used to provide approximate estimates of device SEB tolerance[18]. This source emits high-LET fission fragments and alpha particles. The emitted alpha particles have an energy of 5.9 MeV. About 3% of the emitted ions possess LET values exceeding 40 MeV-cm²/mg. A significant fraction of Cf-252 fission fragments have ranges spanning 3 to 10 μm[18]. The IV characteristics of all devices used in this study are shown in Fig. S4. Some variation is observed from device to device. These kinds of small device-to-device variations are often due to uneven defect/implantation distribution on the wafer. To account for such variability, the devices were selected from different places on the wafer. For the Cf-252 fission fragment irradiation experiments, a sequential test was conducted to check the radiation response by subjecting a pristine P13 device to reverse bias voltages from 300 V to 450 V with 50 V increments. In each full 60 min constant voltage stress, the device underwent a 30 min period of electrical stress without radiation to ensure electrical stability and establish a baseline current. Subsequently, the device was exposed to Cf-252 irradiation while maintaining the bias voltage for the next 30 minutes. Due to the lower flux of fission fragments in Cf-252 irradiation, a longer irradiation time was selected than for the oxygen and chlorine ion irradiations. The device (P3) shown in Fig. 3 experiences SEB at a reverse bias of 450 V approximately 12 min after exposure to Cf-252 fission fragments. During 450 V reverse-bias irradiation, the device ceases to function, as confirmed by the comparison of pre-rad and post-rad IV characteristics in Fig 3(b). This 450 V SEB threshold voltage value corresponds to ~50% of the rated electrical breakdown voltage. No degradation was evident after any irradiation cycle below 450 V, highlighting the device's resilience at lower bias levels and confirming that the observed SEB at 450 V is a single-ion-induced phenomenon[31].

The optical microscope images of the physical damage on the device surface before irradiation (pre-rad), after 400 V reverse bias irradiation (pre-SEB), and after 450 V reverse bias irradiation (post-SEB) are shown in Figs. 3(c) to (e). Following the 400 V irradiation, visible damage appears at the edge of the anode. These damaged regions do not cause any degradation of the device's electrical properties, as depicted in the IV characteristics in Fig. 3(b). Also, the SEM images in Fig 3(f) show that damage is confined to the anode metal and does not extend to the underlying p^{++} GaN layer. This limited scope of damage likely accounts for the negligible effect on the device's electrical properties. There is additional damage at the edge of the HET region, as shown in Fig. S5(c). That can be due to leakage paths at the edge

of the HET region[23,24]. Another device (P11) was tested with Cf -252, starting with 350 V reverse bias. The device died at 350 V around 20 min after exposure to the Cf -252 source in its first irradiation cycle. This result suggests that the lower voltage irradiations do not affect the device and that the device dies from a single ion strike. Furthermore, no edge damage is observed in this device during its 1-hour exposure [see Fig. S5(d) in the supplementary material].

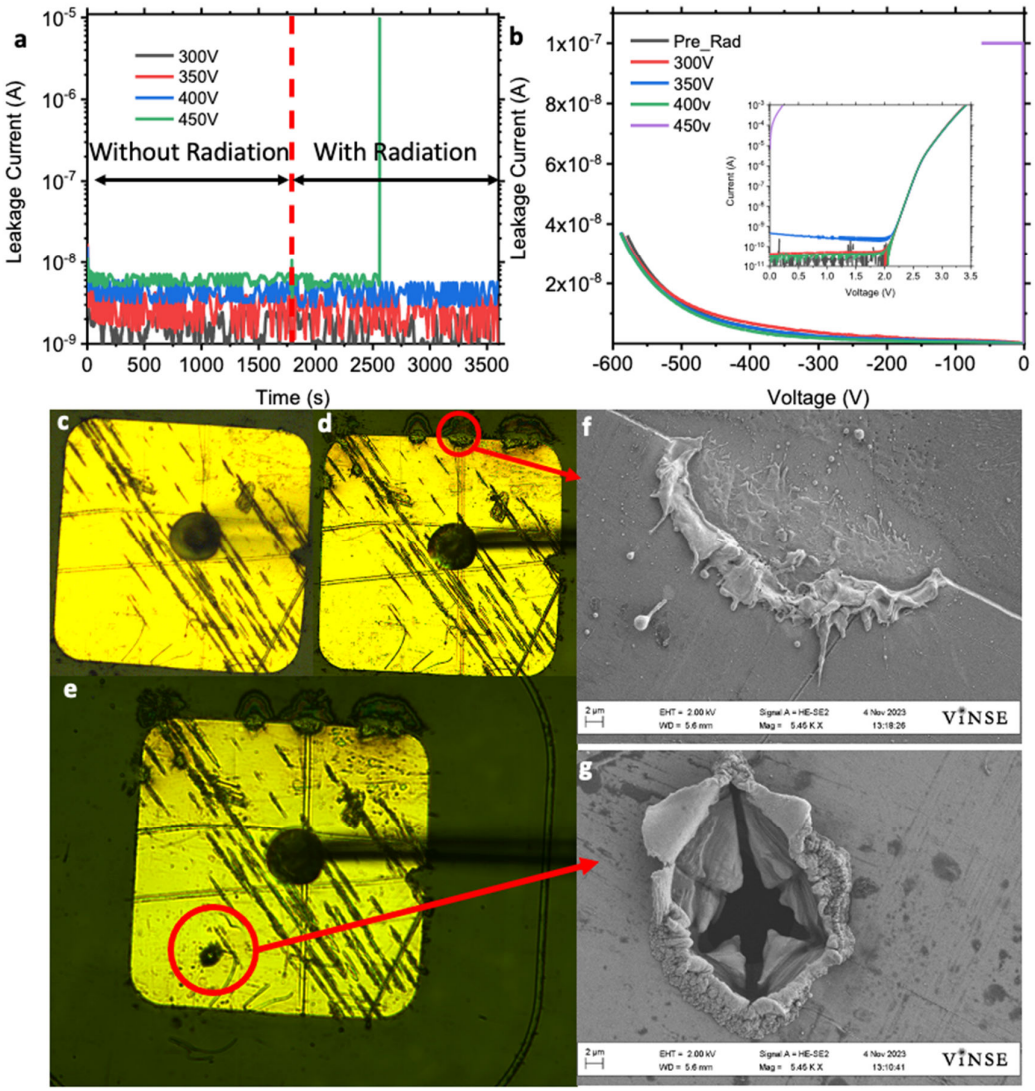

FIG 3: Electrical properties and surface morphology of a GaN PiN diode with HET (device P13) while Cf-252 irradiation: (a) change in leakage current during irradiation in different voltages, (b) optical microscope image of a pristine device, (c) optical microscope image of the device after 400 V reverse bias irradiation (pre-SEB), (d) optical microscope image of the device after 450 V reverse bias irradiation (Post-SEB), (e) SEM images of anode edge damage for the device, and (f) SEM image of the damage at the middle of the device after 450 V reverse bias irradiation (Post-SEB).

The above kinds of edge damage are not observed during oxygen or chlorine ion irradiations for which the total irradiation time is less than 1 hour. Only Cf-252 irradiation leads to such damage, and only after the second or third irradiation cycle, corresponding to two to three hours of constant voltage stress. A device that is biased at 400 V for two hours without radiation shows similar anode edge and HET edge damage [see Fig. S5(a) and (b) in the

supplementary material]. Hence, this damage may arise from electrical overstress (EOS), as opposed to effects induced by radiation[32,33]

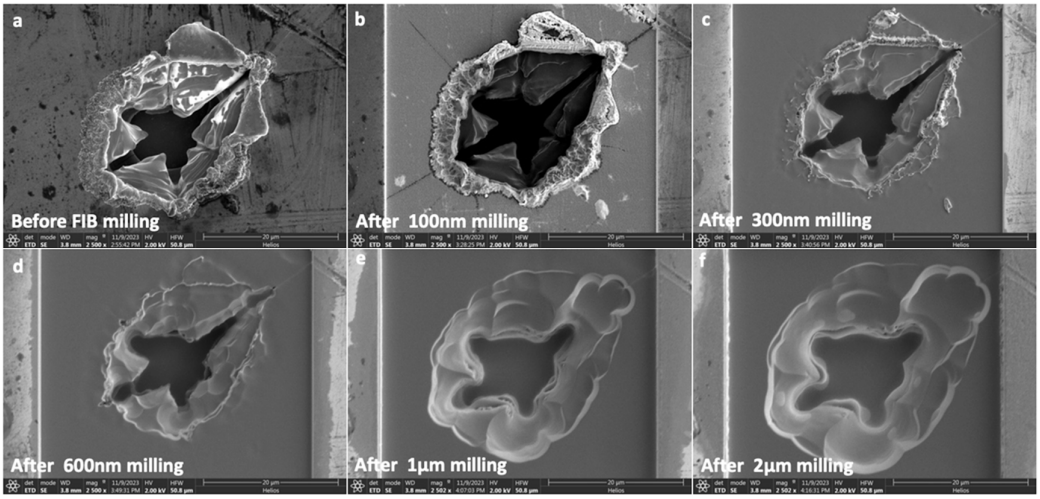

FIG 4: Slice-and-view observations from the surface of a GaN PiN diode with HET using FIB up to ~2 µm depth: (a) SEM image of device surface, and SEM images of the device surface after FIB milling to (b) 100 nm, (c) 300 nm, (d) 600 nm, (e) 1 µm and (f) 2 µm.

Following 450 V irradiation, new damage emerged in the central region of the device, as shown in Fig. 3(e). A detailed examination of this damage is done by an SEM image that clearly illustrates its deeper penetration into the GaN material, as shown in Fig. 3(g) [also, see Fig. S6 in the supplementary material]. Further investigation into this damage was conducted through SEM imaging after FIB milling to various depths. SEM images of the damage at depths of 100 nm to 2 µm after FIB milling are shown in Fig. 4(a) to (f). Even after 2 µm FIB milling, the damage is visible, indicating the depth of this damage is more than 2 µm. Therefore, the damage extends well beyond the PN junction and into the *n*-drift layer, which is around 400 nm below the surface of the device (see Fig. 1). This result shows that bulk damage is the primary cause of device failure, as opposed to damage observed at the edges.

Altogether, five similar devices were tested with the Cf-252 source with breakdown voltages shown in Table SIII in the supplementary material. The average breakdown voltage is 400.0 ± 35.4V, which is around 50% of the rated breakdown voltage. Therefore, these GaN PiN diodes are more vulnerable to Cf -252 fission fragments than oxygen and chlorine ions.
Also, two pristine devices were tested with an Am-241 source, which emits alpha particles at 5.4 MeV, having LET values less than 1 MeV-cm²/mg and ranges greater than 10 µm in GaN[34,18]. The average breakdown voltage is 775.0 ± 35.4 V in air, which is well above the breakdown voltages observed during Cf-252 irradiation and in the range of electrical breakdown voltage. These findings confirm that heavy ions and not alpha particles from the Cf-252 source result in the observed breakdown in Fig. 3.

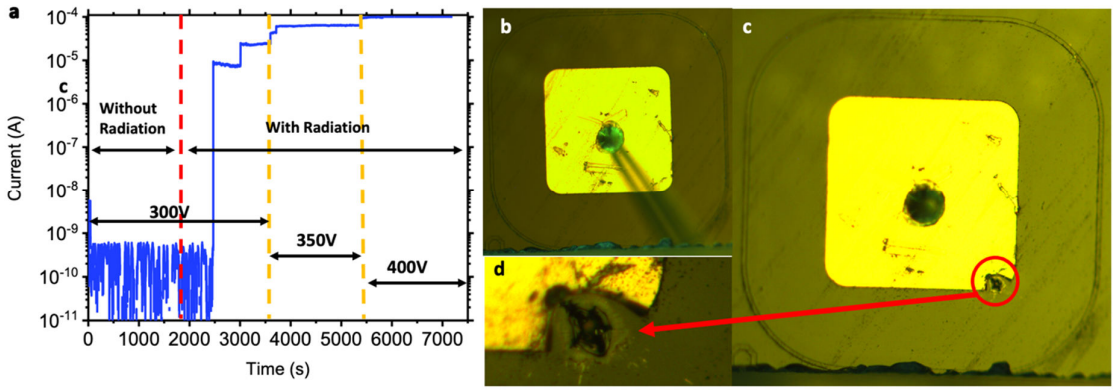

FIG 5: Electrical properties and surface images of a GaN PiN diode with JTE during Cf-252 fission fragment irradiation: (a) change in leakage current during irradiation in different voltages, (b) optical microscope image of a pristine device, (c) optical microscope image of the device after 400 V reverse bias irradiation (post-SEB), (d) magnified optical microscope image of the SEB damage of the device in (c).

Analogous devices featuring the JTE edge termination design also were assessed as baseline devices using a Cf-252 source. The device structure and corresponding current-voltage (IV) characteristics are depicted in Fig. 1(b). The device was biased with a 300 V reverse bias and allowed to stabilize for 30 min to attain a steady-state current. Subsequently, the device was exposed to fission fragments from the Cf-252 source while maintaining the 300 V bias for an additional 30 min. The bias was then increased to 350 V without removing the Cf-252 source, followed by another 30 min waiting period. Further, the bias was raised to 400 V, and shortly after, the leakage current exceeded the compliance current threshold, indicating device failure. Forward and reverse IV characteristics of the device were examined, confirming its non-functionality. Optical microscope inspection of the device surface revealed radiation-induced damage, notably concentrated at the edge of the anode, as illustrated in Figs. 5(c) and (d). This result is consistent with observations in the literature on Ga_2O_3 and SiC Schottky diodes. A similar device underwent similar testing procedures, yielding the same results with radiation damage concentrated at the anode edge, as presented in Fig. S7. These findings affirm that the HET design exhibits superior electric field management at the anode edge compared to the JTE edge termination design. Consequently, the implementation of HET demonstrates the potential to reduce the radiation sensitivity at the anode edge, highlighting its efficacy in radiation-hardened device designs. A complete discussion of the effectiveness of JTE edge termination and the effect of anode thickness and anode doping level will be published elsewhere.

Finally, the supplementary material contains information on the pre-irradiation IV characteristics of all HET devices used in this study (Fig. S1, S2, and S4). The breakdown voltages of devices P1, P2, P3, and P4 under oxygen ion irradiation (Table SI), electrical characterization for chlorine ion irradiated devices (Fig. S3), breakdown voltages of the devices under chlorine ion irradiation (Table SII), optical images of the devices that show SEB in the first irradiation cycle and the devices stressed without radiation (Fig. S5(d)), breakdown voltages of the devices irradiated with Cf-252 fission fragments (Table SIII), and SEM images of the SEB damage in the device in Fig.3 from different angles (Fig. S6) and optical microscope image radiation damage of another device that has JTE edge termination.

In summary, the present study assessed homojunction GaN vertical PiN diodes with HET, subjecting them to oxygen, chlorine, Cf-252 fission fragments, and alpha particles from Am-241 source irradiations. No observable radiation-induced damage occurred with oxygen and chlorine ions, attributable to their lower LET and range within GaN. However, Cf-252 fission fragments reduce the breakdown voltage to approximately 50% of the experimental

electrical breakdown voltage in the absence of ion irradiation. This outcome is attributed to higher-LET and higher-range ions present in the Cf-252 fission-fragment irradiation. Furthermore, optical-microscope and SEM analysis revealed that radiation damage is localized in the central region of the device rather than in the edge of the anode, contrary to common observations in wide-bandgap devices in the literature and baseline devices in this study, which contains JTE edge termination instead of HET. These devices showed radiation-induced damage in the edge of the anode, similar to the Ga_2O_3 and SiC devices in the literature. This result suggests that the hybrid-edge-termination design mitigates radiation sensitivity at the anode edge region by reducing electric field crowding in that area.

The present research was supported by the Air Force Center of Excellence in Radiation Effects, award No FA9550-22-1-0012, and the Office of Naval Research (ONR), award No N00014-23-1-2676. J.D.C. acknowledges support from the Department of Energy, Basic Energy Sciences under grant No DE-FG02-09ER46554. The assistance and technical expertise of the staff at Vanderbilt Institute for Space and Defense Electronics (ISDE) and Vanderbilt Institute of Nanoscale Science and Engineering (VINSE) were invaluable to the success of this work.

The work at Sandia was performed under the ARPA-E OPEN+ Kilovolt Devices Cohort, directed by Dr. Isik Kizilylli. Sandia National Laboratories is a multi-mission laboratory managed and operated by National Technology & Engineering Solutions of Sandia, LLC, a wholly owned subsidiary of Honeywell International Inc., for the U.S. Department of Energy's National Nuclear Security Administration under contract DE-NA0003525.

AUTHOR DECLARATION

The authors have no conflict to disclose.

DATA AVAILABILITY

The data that support the findings of this study are available from the corresponding author upon reasonable request.

REFERENCES

[1] J. Y. Tsao, S. Chowdhury, M. A. Hollis, D. Jena, N. M. Johnson, K. A. Jones, R. J. Kaplar, S. Rajan, C. G. Van de Walle, E. Bellotti, C. L. Chua, R. Collazo, M. E. Coltrin, J. A. Cooper, K. R. Evans, S. Graham, T. A. Grotjohn, E. R. Heller, M. Higashiwaki, M. S. Islam, P. W. Juodawlkis, M. A. Khan, A. D. Koehler, J. H. Leach, U. K. Mishra, R. J. Nemanich, R. C. N. Pilawa-Podgurski, J. B. Shealy, Z. Sitar, M. J. Tadjer, A. F. Witulski, M. Wraback, and J. A. Simmons, Adv. Electron Mater. **4**, 1600501 (2018).

[2] N. Islam, M. F. P. Mohamed, M. F. A. J. Khan, S. Falina, H. Kawarada, and M. Syamsul, Crystals **12**, 1581 (2022).

[3] T. J. Flack, B. N. Pushpakaran, and S. B. Bayne, J. Electron Mater. **45**, 2673 (2016).

[4] H. Hanawa, Y. Satoh, and K. Horio, Microelectron Eng. **147**, 96 (2015).

[5] R. C. Sharma, R. Nandal, N. Tanwar, R. Yadav, J. Bhardwaj, and A. Verma, J. Phys.: Conf. Ser. **26**, 012008 (2023).

[6] A.Y. Polyakov, S.J. Pearton, P. Frenzer, F. Ren, L. Liu, and J. Kim, J. Mater. Chem. C Mater. 877–887 (2013).

[7] S. Yuvaraja, V. Khandelwal, X. Tang, and X. Li, Chip, 100072 (2023), in press.

[8] L. Z. Scheick, IEEE Radiation Effects Data Workshop, Portland, OR July 11-15 (IEEE, 2016), pp. 36-41.

[9] S. J. Pearton, A. Haque, A. Khachatrian, A. Ildefonso, L. Chernyak, and F. Ren, ECS J. Solid-State Sci. Technol. **10**, 075004 (2021).

[10] H. Amano, Y. Baines, E. Beam, M. Borga, T. Bouchet, P. R. Chalker, M. Charles, K. J. Chen, N. Chowdhury, R. Chu, C. De Santi, M. M. De Souza, S. Decoutere, L. Di Cioccio, B. Eckardt, T. Egawa, P. Fay, J. J. Freedsman, L. Guido, O. Häberlen, G. Haynes, T. Heckel, D. Hemakumara, P. Houston, J. Hu, M. Hua, Q. Huang, A. Huang, S. Jiang, H. Kawai, D. Kinzer, M. Kuball, A. Kumar, K. B. Lee, X. Li, D. Marcon, M. März, R. McCarthy, G. Meneghesso, M. Meneghini, E. Morvan, A. Nakajima, E. M. S. Narayanan, S. Oliver, T. Palacios, D. Piedra, M. Plissonnier, R. Reddy, M. Sun, I. Thayne, A. Torres, N. Trivellin, V. Unni, M. J. Uren, M. Van Hove, D. J. Wallis, J. Wang, J. Xie, S. Yagi, S. Yang, C. Youtsey, R. Yu, E. Zanoni, S. Zeltner, and Y. Zhang, J. Phys. D: Appl. Phys. **51**, 163001 (2018).

[11] K. Mukherjee, C. De Santi, M. Borga, K. Geens, S. You, B. Bakeroot, S. Decoutere, P. Diehle, S. Hübner, F. Altmann, M. Buffalo, G. Meneghesso, E. Zanoni, and M. Meneghini, Materials **14**, 2316 (2021).

[12] K. Motoki, T. Okahisa, S. Nakahata, N. Matsumoto, H. Kimura, H. Kasai, K. Takemoto, K. Uematsu, M. Ueno, Y. Kumagai, A. Koukitu, and H. Seki, Journal of Crystal Growth **237**, 912 (2002).

[13] D. M. Fleetwood, E. X. Zhang, R. D. Schrimpf, and S. T. Pantelides, IEEE Trans. Nucl. Sci. **69**, 1105 (2022).

[14] S. You, K. Geens, M. Borga, H. Liang, H. Hahn, D. Fahle, M. Heuken, K. Mukherjee, C. De Santi, M. Meneghini, E. Zanoni, M. Berg, P. Ramvall, A. Kumar, M.T. Björk, B. J. Ohlsson, and S. Decoutere, Microelectronics Reliability **126**, 114218 (2021).

[15] R. Kucharski, T. Sochacki, B. Lucznik and Y. Otoki, J. Applied Physics **128**, 050902(2020).

[16] A. Sengupta, D. R. Ball, A. L. Sternberg, S. Islam, A. S. Senarath, R. A. Reed, M. W. McCurdy, E. X. Zhang, J. M. Hutson, M. L. Alles, J. M. Osheroff, B. Jacob, C. W. Hitchcock, S. Goswami, R. D. Schrimpf, K. F. Galloway, and A. F. Witulski, IEEE Trans. Nucl. Sci., accepted. Available via early access, doi:10.1109/TNS.2024.3357129.

[17] J. S. George, R. Koga, R. M. Moision and A. Arroyo, 2013 IEEE Radiation Effects Data Workshop (REDW), San Francisco, CA, July 8 – 12 (IEEE, 2013), pp 167-174.

[18] J. L. Titus, IEEE Trans. Nucl. Sci. **60**, 1912 (2013).

[19] R. M. Cadena, D. R. Ball, E. X. Zhang, S. Islam, A. Senarath, M. W. McCurdy, E. Farzana, J. S. Speck, N. Karom, A. O'Hara, B. R. Tuttle, S. T. Pantelides, A. F. Witulski, K. F. Galloway, M. L. Alles, R. A. Reed, D. M. Fleetwood, and R. D. Schrimpf, IEEE Trans. Nucl. Sci. **70**, 363 (2023).

[20] T. Shoji, S. Nishida, K. Hamada, and H. Tadano, Microelectronics Reliability **55**, 1517 (2015).

[21] T. Nelson, P. Pandey, D. G. Georgiev, M. R. Hontz, A. D. Koehler, K. D. Hobart, T. J. Anderson, A. Ildefonso, and R. Khanna, IEEE Trans. Electron Devices **14**, 2005 (2022).

[22] T. Nelson, P. Pandey, D. G. Georgiev, R. Khanna, M. R. Hontz, A. G. Jacobs, J. C. Gallagher, A. D. Koehler, K. D. Hobart, and T. J. Anderson, 2023 Workshop on Wide Bandgap Power Devices and Applications (WiPDA), Dayton, OH, Nov 4-6 (IEEE, 2023).

[23] M. P. King, A. M. Armstrong, J. R. Dickerson, G. Vizkelethy, R. M. Fleming, J. Campbell, W. R. Wampler, I. C. Kizilyalli, D. P. Bour, O. Aktas, H. Nie, D. Disney, J. Wierer, A. A. Allerman, M. W. Moseley, F. Leonard, A. A. Talin, and R. J. Kaplar, IEEE Trans. Nucl. Sci. **62**, 2912 (2015).

[24] M. A. Ebrish, M. A. Porter, A. G. Jacobs, J. C. Gallagher, R. J. Kaplar, B. P. Gunning, K. D. Hobart, and T. J. Anderson, Crystals **12**, 623 (2022).

[25] M. A. Ebrish, M. Porter, A. Jacobs, J. C. Gallagher, R. J. Kaplar, B. P. Gunning, K. D. Hobart, and T. J. Anderson, Applied Physics Express **16**, 116501 (2023).

[26] S. Islam, A. S. Senarath, A. Sengupta, E. X. Zhang, D. R. Ball, D. M. Fleetwood, R. D. Schrimpf, E. Farzana, A. Bhattacharyya, N. S. Hendricks, and J. S. Speck, 2023 Device Research Conference (DRC), Santa Barbara, CA, June 25-28 (IEEE, 2023), pp. 20-21.

[27] E. C. Stone, R. E. Vogt, F. B. McDonald, B. J. Teegarden, J. H. Trainor, J. R. Jokipii, and W. R. Webber, Space Sci. Rev. **21**, 355 (1977).
[28] A. Omerbegovii, Ö. Aydogar, K. Schwingenshuh, and R. Harboe-Sørensen, RPC MAG / ROSETTA ESA project, Graz, Austria, Nov. (1999), pp 3-4.
[29] J. T. Blandford and J. C. Pickel, IEEE Trans. Nucl. Sci. **32**, 4282 (1985).
[30] SRIM – Stopping and Range of Ions in Matter. https://srim.org/, accessed 21 Nov 2023.
[31] G. H. Johnson, J. H. Hohl, R. D. Schrimpf, and K. F. Galloway, IEEE Trans. Electron Devices **40**, 1001 (1991).
[32] D. Mueller, C. Fella, F. Altmann, J. Graetz, A. Balles, M. Ring, and J. Gambino, Microelectronics Reliability **135**, 114589 (2022).
[33] S. Kayali, Basic Failure Modes and Mechanisms (JPL NASA, 1997), pp. 89-108.
[34] A. Sandupatla, S. Arulkumaran, N. G. Ing, S. Nitta, J. Kennedy, and H. Amano, Micromachines **11**, 519 (2020).